nature COMMUNICATIONS

ARTICLE

Received 4 Jan 2013 | Accepted 21 May 2013 | Published 26 Jun 2013

DOI: 10.1038/ncomms3040

Coherent topological transport on the surface of Bi_2Se_3

Dohun Kim[1], Paul Syers[1], Nicholas P. Butch[2], Johnpierre Paglione[1] & Michael S. Fuhrer[1,3]

The two-dimensional surface of the three-dimensional topological insulator is in the symplectic universality class and should exhibit perfect weak antilocalization reflected in positive weak-field magneto-resistance. Previous studies in topological insulator thin films suffer from high level of bulk *n*-type doping making quantitative analysis of weak antilocalization difficult. Here we measure the magneto-resistance of bulk-insulating Bi_2Se_3 thin films as a function of film thickness and gate-tuned carrier density. For thick samples, the magnitude of weak antilocalization indicates two decoupled (top and bottom) symplectic surfaces. On reducing thickness, we observe first a crossover to a single symplectic channel, indicating coherent coupling of top and bottom surfaces via interlayer tunnelling, and second, a complete suppression of weak antilocalization. The first crossover is governed by the ratio of phase coherence time to the inter-surface tunnelling time, and the second crossover occurs when the hybridization gap becomes comparable to the disorder strength.

[1] Department of Physics, Center for Nanophysics and Advanced Materials, University of Maryland, College Park, Maryland 20742-4111, USA. [2] Condensed Matter and Materials Division, Lawrence Livermore National Laboratory, Livermore, California 94550, USA. [3] School of Physics, Monash University, Victoria 3800, Australia. Correspondence and requests for materials should be addressed to M.S.F. (email: michael.fuhrer@monash.edu).

© 2013 Macmillan Publishers Limited. All rights reserved.

Weak localization (WL) and weak antilocalization (WAL) describe corrections to the classical electrical conductivity of two-dimensional (2D) electron gases due to coherent interference of time-reversed paths. The 2D surface state of the three-dimensional strong topological insulator (TI) is fundamentally distinct from other 2D electron systems[1] in that the Fermi arc encircles an odd number of Dirac points[2–8]. The TI surface is in the symplectic universality class and uniquely among 2D systems remains metallic and cannot be localized by (time-reversal symmetric) disorder[9]. In the absence of localization, the TI surface state is expected to exhibit perfect WAL described by, Hikami *et al.*[10]:

$$\Delta\sigma(H) = \alpha\frac{e^2}{\pi h}\left[\ln\frac{H_0}{H} - \psi\left(\frac{1}{2}+\frac{H_0}{H}\right)\right] \quad (1)$$

where $H_0 = \hbar/4De\tau_\varphi$ is a characteristic field related to the phase coherence time τ_φ and diffusion constant D, ψ is the digamma function, and α is the overall amplitude whose expected value for a single 2D channel is 1/2. However, WAL is sensitive to the competition between the phase coherence time τ_φ and other time scales[11]; in TI thin films, carriers may scatter into additional conducting channels (from top to bottom surface, or into the conducting bulk). Moreover, in finite-size samples inter-surface coupling can destroy the topological protection[12–14], modifying the WAL behaviour. The question arises: at what size can a thin TI sample be treated as having decoupled topological surface states?

In contrast to previous studies of WAL in TI thin films[15–22] where strong surface to bulk scattering dominates inter-channel coupling, here we report WAL measurements in gate-tuned, bulk-insulating Bi_2Se_3 thin films where we expect negligible surface-bulk scattering. We find that the WAL behaviour in TI regime is governed by the ratio of τ_φ to the inter-surface tunnelling time $\tau_t = h/2\Delta$, where h is Planck's constant and Δ is the hybridization gap induced by inter-surface tunnelling[12,14]. For thick films (17 nm), $\tau_\varphi/\tau_t < 1$ and we observe the signature of a true 2D topological metal: perfect WAL according to equation (1) with $\alpha = ½ + ½ = 1$ corresponding to two decoupled TI surfaces each with $\alpha = ½$. A thickness and doping-dependent crossover is observed when $\tau_\varphi/\tau_t > 1$ to a regime where $\alpha = ½$, indicating the coherent coupling of two TI surfaces. The result indicates that WAL is extraordinarily sensitive to sub-meV coupling between top and bottom topological surfaces, and the surfaces of a TI film may be coherently coupled even for thicknesses as large as 12 nm. For even thinner samples, Δ becomes comparable to the disorder strength and the Berry's phase is completely randomized at low carrier density causing the suppression of WAL and WL, reflecting the loss of topological protection for strongly coupled surfaces.

Results

Characterization of Bi_2Se_3 Hall bar devices. We study mechanically exfoliated Bi_2Se_3 single crystals[23] ranging in thickness from 5 to 17 quintuple layers (QL). Figure 1a shows a representative device (thickness 12 QL), where height profiles across the width direction of the 17, 12, 7 and 5 QL devices are shown in Fig. 1b. In order to achieve the topological transport regime, we employed molecular charge transfer *p*-type doping by thermal evaporation of 2,3,5,6-tetrafluoro-7,7,8,8-tetracyano quinodimethane, described previously[24] (see also Methods, Supplementary Fig. S1, and Supplementary Note 1).

Figure 1c,d show the longitudinal resistivity ρ_{xx} and Hall carrier density $n_H = 1/(eR_H)$ (where R_H is the Hall coefficient, and e is the elementary charge) of the devices at a temperature of 2 K as a function of back gate voltage V_g. We measure n_H in the range of 2–7 × 10^{12} cm^{-2} at zero gate voltage. The carrier density in the topological surface state at the bulk conduction band edge is ~0.8–1.0 × 10^{13} cm^{-2}, hence the devices are close to the TI regime before application of a back gate voltage. Ambipolar electric field effects are indicated by the sharp peak of $\rho_{xx}(V_g)$ and the sign change in n_H at the charge neutrality points ($V_{g,0}$, Fig. 1c dashed lines). The dependence of $\rho_{xx}(V_{g,0})$ on temperature T in all of our devices, including 5 QL, shows metallic behaviour (see Supplementary Fig. S2), which is likely due to conduction through inhomogeneity-driven electron-hole puddles[24,25]. However, the thinnest (5 QL) device shows an anomalously large maximum $\rho_{xx}(V_{g,0})$ of about 23 kΩ, which cannot be understood within the self-consistent theory for a Dirac band in the

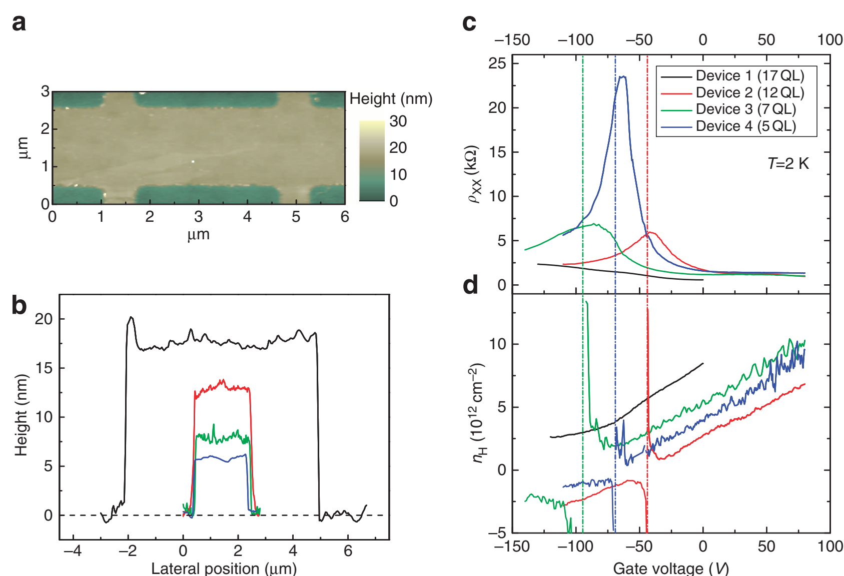

Figure 1 | Characterization of Bi_2Se_3 Hall bar devices. (**a**) Atomic force microscopy image of 12 QL Bi_2Se_3 Hall bar device. (**b**) Height profiles along width directions of the devices used in this study. (**c**) Longitudinal resistivity ρ_{xx} and (**d**) sheet carrier density n_H determined from Hall measurement as a function of back gate voltage at the temperature of 2 K for 17 (black), 12 (red), 7 (green) and 5 (blue) QL devices. The dashed lines show charge neutrality points.

© 2013 Macmillan Publishers Limited. All rights reserved.

presence of charge disorder[24,26,27], suggesting that the inter-surface hybridization gap Δ becomes important in determining the resistivity in this regime[12]. We note that true insulating behaviour (divergent ρ_{xx} as $T\rightarrow 0$) is not observed for the 5 QL sample, but was previously observed for 3 QL Bi_2Se_3 (ref. 13). More work is needed to understand the ρ_{xx} maximum in the 5 QL sample (see Supplementary Note 2 for further discussion).

WAL in the topological transport regime. We now turn to discuss gate-tuned WAL behaviour in the TI regime. Figure 2 shows the magneto-conductivity $\Delta\sigma(H)$ for all four devices. Curves are taken at similar carrier density $n = C_g(V_g - V_{g,0})/e$ (where gate capacitance $C_g \approx 11$ nFcm^{-2}) ranging from $\approx 7\times 10^{12}$ cm^{-2} (n-type) to -2×10^{12} cm^{-2} (p-type) except for the 17 QL device where only n-type carrier density (7 and 2×10^{12} cm^{-2}) could be observed due to relatively high initial doping. The data for the entire range of n and thickness can be fitted (dashed curves in Fig. 2) well with equation (1). The validity of equation (1) in the multichannel limit has been addressed in a number of previous studies[16,19,20,28], finding that equation (1), in particular the logarithmic correction term, provides a robust physical description of WAL behaviour even in the multichannel limit irrespective of the Drude conductivity of each channel[20,28]. Therefore, $\alpha = m/2$ probes the number of channels m. Moreover, although crossover to WL was predicted[29] in a gapped TI thin films (considered single 2D channel), further study of WAL in multi-channels including coherent coupling between channels[28], as well as experimental observation in molecular beam epitaxy grown Bi_2Se_3 (ref. 22) points out that WL can be neglected down to $\sim$5 QL thickness. Our samples thus lie in the regime of dominant WAL.

Coupling of coherent transport in Bi_2Se_3 surface states. Figure 3 shows the variation of α obtained from the fit to equation (1) as a function of n for 17 (black), 12 (red), 7 (green) and 5 (blue) QL devices measured at 2 K. In all devices α is close to 1/2 at high $n \approx 8\times 10^{12}$ cm^{-2}, which we interpret as WAL in a single strongly coupled coherent channel[15–17,19,20] in the presence of surface to bulk scattering, as bulk states becomes energetically accessible (non-TI regime). Thus, we restrict the carrier density ranging $n < 6\times 10^{12}$ cm^{-2} for investigating WAL behaviours in TI regime. The dependence of α on gate tuning shows very different behaviours depending on the thickness of the devices. The thickest device (17 QL) shows WAL consistent with two decoupled top and bottom topological surfaces ($\alpha \approx 1$) starting at moderate $n \approx 6\times 10^{12}$ cm^{-2}, maintained down to the minimum accessible n. Similar variation of α ranging from 0.7 to 1 was observed in Steinberg *et al.*[20], with the application of top gate, and interpreted there as the decoupling of top surface and bulk (plus bottom) channels due to formation of band-bending-induced depletion layer. We do not rule out the possible contribution of bulk-surface scattering in 17 QL at high n. However, we note that this effect alone cannot explain the general behaviour of α for low n and thinner devices. Notably, we identify two crossovers in the 12 QL device: we observe sharp transition of α from $\approx 1/2$ to ≈ 1 near $n \approx 1\times 10^{12}$ cm^{-2} (n-type), and back to 1/2 at $n \approx -1\times 10^{12}$ cm^{-2} (p-type). $\Delta\sigma(H)$ in our devices include a moderate contribution from (universal) conductance fluctuations (Fig. 2), as commonly observed in micro-fabricated Bi_2Se_3 devices[16,21]; the fluctuations are reduced by fitting to equation (1) over a large field range (0 T, 0.8 T). At the upper end of this field range, the magnetic length $l_B = (\hbar/eH)^{1/2}$ becomes comparable to the electronic mean free path l_{mfp}, approaching the regime where equation (1) may not be valid. However, we verified that the effect of increasing the field fitting range from (0 T, 0.02 T), where $l_B >> l_{mfp}$, to (0 T, 1 T), where $l_B \gtrsim l_{mfp}$, is only to reduce the fluctuations in α, without changing the average value, and that conductance fluctuations result in variation in α <0.1 in a given thermal run (see Supplementary Fig. S3c and Supplementary Note 3). Moreover, we repeated similar WAL measurements at 2 K for the 12 QL device on five different thermal runs, where the conductance fluctuation contribution is randomized, and find that the crossovers are reproducible within the experimental uncertainty represented by the standard deviation determined from the repetitive measurements (Fig. 3, error bars). This transition is absent in the 7 QL device, where WAL in the entire range of n indicates a strongly coupled single channel ($\alpha \approx 1/2$). Finally, at an even smaller thickness (5 QL), we observe strong suppression of WAL for -1×10^{12} cm^{-2} < n < 1×10^{12} cm^{-2}, (inset of Fig. 3, see also Fig. 2d).

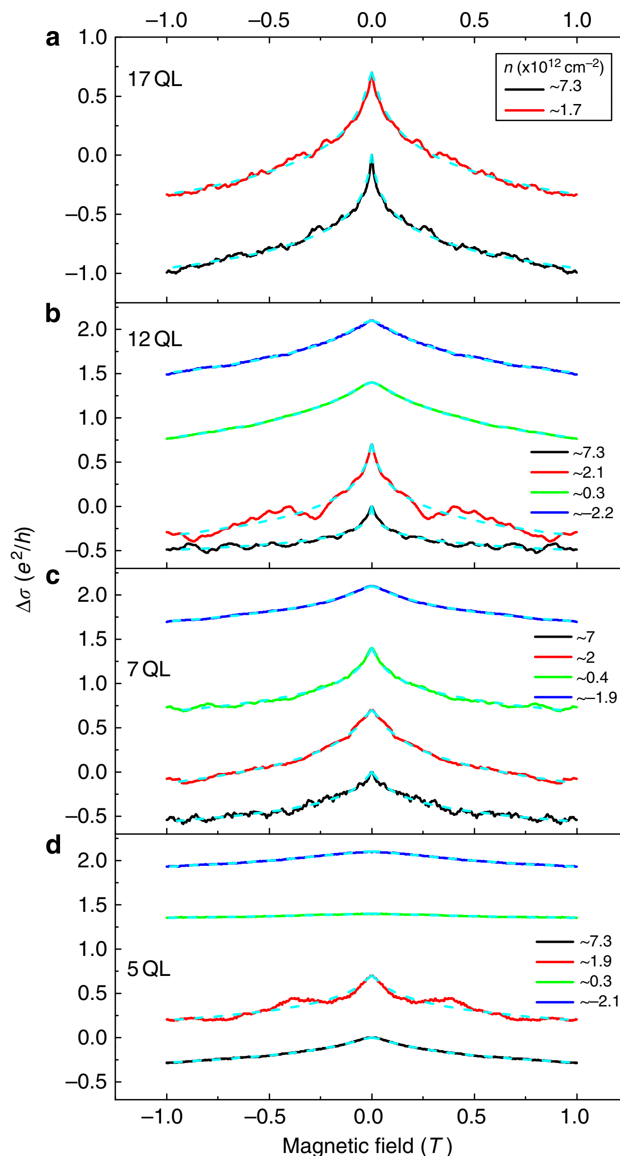

Figure 2 | WAL in the TI regime. Magneto-conductivity $\Delta\sigma$ as a function of perpendicular magnetic field H in (**a**), 17, (**b**), 12, (**c**), 7 and (**d**), 5 QL devices measured at 2 K at gate-induced carrier densities indicated in the legends. Dashed curves show least-square fits to equation (1). Zeros of all curves are offset by 0.7 e^2/h for clarity.

© 2013 Macmillan Publishers Limited. All rights reserved.

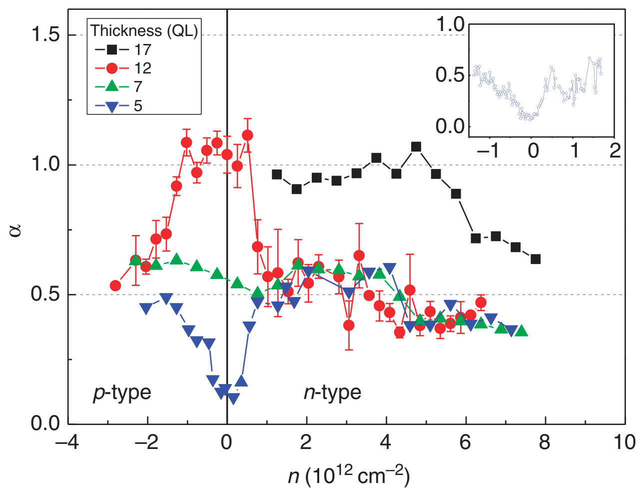

Figure 3 | Coupling of coherent transport in Bi_2Se_3 surface states. Variation of the amplitude of WAL α as a function of 2D carrier density n for 17 (black square), 12 (red circle), 7 (green triangle) and 5 QL (blue triangle) thick devices measured at 2 K. For the 12 QL device, the error bars show standard deviations determined from WAL measurements taken at five different thermal runs. The inset shows detailed behaviour of suppression of WAL for 5 QL at small n.

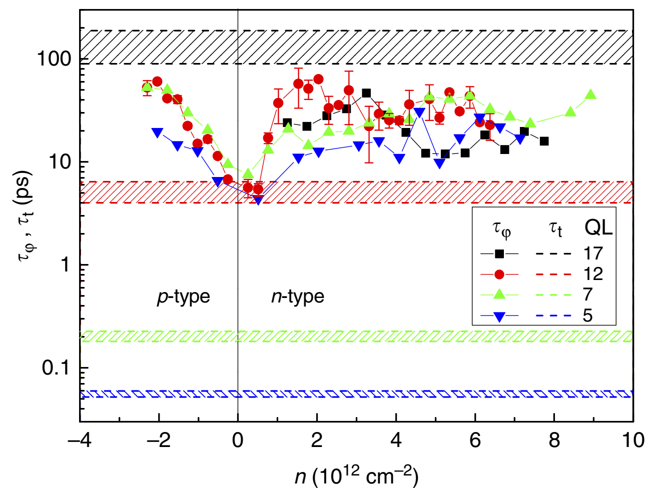

Figure 4 | Phase coherence time versus interlayer tunnelling time. Comparison of phase coherence time, τ_φ, determined from fit to equation (1) and transport scattering time to interlayer tunnelling time, τ_t, estimated from surface hybridization induced energy gap Δ as a function of 2D carrier density n. Symbols are experimentally measured τ_φ for 17 (black square), 12 (red circle), 7 (green triangle) and 5 QL (blue triangle) devices. The hatched areas with corresponding colours show estimated windows of inter-surface tunnelling time τ_t.

Phase coherence time versus inter-surface tunnelling time. We now examine the coherence time τ_φ and compare with the estimated interlayer tunnel time τ_t. We estimate $\tau_\varphi = \hbar/4eDH_0$ from the fits to equation (1) and using $D = \tau\, v_F^2/2$ where Fermi velocity $v_F \approx 3\times10^7\,\mathrm{cm\,s^{-1}}$ for Bi_2Se_3 (ref. 30), and the momentum relaxation time τ is calculated from the measured $\sigma(n)$. τ_t represents the characteristic time of transition (half the period Rabi oscillations) between localized states in two quantum wells with energy splitting Δ, thus $\tau_t = h/2\Delta$. We estimate Δ in Bi_2Se_3 by fitting the existing experimental data[12] to an exponentially decaying function. We estimated the range of $\Delta(t)$ by including (1) sizable Δ in 2,3,4 and 5 QL (upper bound) and (2) all data from 2 to 8 QL (lower bound) in the fit and obtained $\Delta(t) = [992\,\mathrm{meV}]e^{-0.67[t\,(\mathrm{nm})]}$ and $\Delta(t) = [879\,\mathrm{meV}]e^{-0.62[t\ (\mathrm{nm})]}$. The resultant range of Δ is 34.8–39.5, 9.1–11.44, 0.32–0.51 and 0.01–0.02 meV for 5, 7, 12 and 17 QL, respectively. (Theoretical calculations of finite-size effects in Bi_2Se_3 predict systematically smaller Δ at a given thickness and also suggest that Δ shows oscillatory decaying behaviour[14], which do not seem to be observed in the previous work[12] or this work.)

Figure 4 shows the estimated τ_φ (symbols) and τ_t (hatched areas) as functions of n for the different thickness samples. Upon gate tuning, τ_φ changes by an order of magnitude ranging from $\approx$4 to $\approx$50 ps, and shows a sharp dip near $n = 0$. For the 17 QL device, $\tau_\varphi/\tau_t < 1$ in the entire range of n. In this limit, electrons on either surface lose coherence before scattering to the other, thus each surface acts as an independent coherent transport channel and $\alpha \approx 1$. In contrast, a crossover occurs from $\tau_\varphi/\tau_t >> 1$ at high unipolar n- and p-type carrier densities to $\tau_\varphi/\tau_t < 1$ near $n = 0$ in the 12 QL device, which is consistent with the observed crossover from $\alpha = ½$ to $\alpha = 1$ (Fig. 3). In the thinner device (7 QL), the condition $\tau_\varphi/\tau_t >> 1$ is satisfied, and the two surfaces are strongly coupled ($\alpha \approx 1/2$) for the entire range of n. The systematic tuning from coherent coupled to decoupled regimes upon variation of τ_φ/τ_t confirms that interlayer tunnelling is the primary coherent coupling mechanism in the TI regime. As τ_t is primarily determined from the thickness of Bi_2Se_3 thin films, whereas τ_φ can vary significantly depending on the sample quality, we expect that the decoupling crossover thickness is not universal but can occur in different thickness if the surface phase coherence can be modified. For instance, decreasing phase coherence of the surface electrons by addition of magnetic impurities[31] should result in a reduced critical thickness above which decoupled coherent transport can be observed. In principle, temperature-dependent dephasing offers an additional opportunity to tune from coupled to decoupled surfaces. However, we observe weak dependence of the coherence time on temperature (see Supplementary Fig. S4 and Supplementary Note 4), which limits temperature as a parameter to control interlayer coherence. The weak temperature dependence of τ_φ is observed elsewhere[21] but not understood, though it suggests an extrinsic mechanism. If the low-temperature decoherence can be improved, it may be possible to explore temperature-driven coherent coupling/decoupling of the TI surfaces.

The behaviour described above is in general consistent in the 5 QL device except near the Dirac point, where WAL is strongly suppressed. The suppression of WAL can be understood in terms of the expected change of Berry phase $\theta_B = \pi(1 - \Delta/2E_F)$ in TIs[29,32] as a function of Δ and the Fermi energy E_F; θ_B is reduced from π when hybridization induced gap opens. Assuming a gapped Dirac dispersion $E_F = \sqrt{(\hbar v_F k_F)^2 + (\Delta/2)^2}$, we estimate $E_F \le 52$ meV and $\theta_B \le 0.67\pi$ at $|n| \le 1\times10^{12}\,\mathrm{cm^{-2}}$. This range of n is comparable to the electron-hole puddle density $n^* \approx 0.5\times10^{12}\,\mathrm{cm^{-2}}$ per surface (Fig. 1d), hence transport occurs through a landscape of electron and hole puddles with θ_B spanning the entire range $0 \le \theta_B \le \pi$. It appears that in this regime of highly inhomogeneous Berry phase that both WAL and WL (expected as $\theta_B \to 0$) are suppressed.

Discussion

In contrast to semi-classical Boltzmann transport in Bi_2Se_3 TI films, where the signature of finite-size effect appear only in the ultrathin limit ($\le$ 3 QL) (ref. 13), phase coherent transport offers an exquisitely sensitive probe of the hybridization of top and bottom transport channels, detecting a gap Δ as small as 0.3 meV

© 2013 Macmillan Publishers Limited. All rights reserved.

in the 12 QL TI film[12], as well as destruction of topological protection in the few QL film. We note that similar suppression of WAL was recently observed in thin epitaxial Bi_2Se_3 of varying thickness (and Δ) but fixed E_F (ref. 22), and a competition between WAL and WL was observed in gated 4 QL epitaxial $(Bi_{0.57}Sb_{0.43})_2Te_3$ (ref. 33). Our observation of the WAL by tuning both E_F and Δ (thickness) allows us to identify the ratio of τ_φ/τ_t as the driver for the crossover between coupled and decoupled surfaces, and the ratio of Δ to disorder strength as the driver for the crossover to the regime of suppressed WAL/WL. We expect that our results are important in identifying the regimes of carrier density and film thickness in which effects related to topological coherent transport can be observed in thin TI films.

Methods

Bi_2Se_3 field effect transistor fabrication. Low-doped (carrier density $\sim 10^{17}$ cm^{-3}) bulk Bi_2Se_3 single crystals with bulk resistivity exceeding 2 mΩ cm^{-1} at 300 K were grown by melting high purity bismuth (6N) and selenium (5N) in sealed quartz ampoules[23]. Crystals were exfoliated with Scotch tape and deposited on doped Si covered with 300 nm SiO_2. Thin Bi_2Se_3 crystals with thickness ranging from 5 to 17 nm were identified by combined use of optical and atomic force microscopy. From the atomic force microscopy height profile of Bi_2Se_3 thin flakes, atomically flat surfaces with height variation <1 QL were chosen as channel area. Electron beam lithography, thermal evaporation and liftoff techniques were used to make electrical contact (Cr/Au: 5/70 nm). For accurate determination of the geometric factor, thin films were patterned into Hall bar geometry (see Fig. 1a) with typical aspect ratio (L/W) of about 2 and shortest length exceeding 2 µm using Ar plasma at a pressure of ~ 6.7 Pa (5×10^{-2} Torr). Molecular charge transfer doping was done by thermal evaporation of ~ 10 nm of 2,3,5,6-tetrafluoro-7,7,8,8-tetracyanoquinodimethane organic molecules (Aldrich) on top of the fabricated samples[24].

Measurement. Transport measurements were performed using standard four-probe ac methods with low frequency (<17 Hz) excitation currents (r.m.s. amplitude 100 nA) using Stanford Research Systems SR830 Lock in amplifiers and a commercial cryostat equipped with 9 T superconducting magnet. For the 12 QL device, five different WAL measurements as a function of gate voltage at 2 K were conducted, where the sample was warmed up to 300 K and exposed to air for a few hours between thermal runs.

References

1. Novoselov, K. S. *et al.* Two-dimensional gas of massless Dirac fermions in graphene. *Nature* **438,** 197–200 (2005).
2. Qi, X. L. & Zhang, S. -C. Topological insulators and superconductors. *Rev. Mod. Phys.* **83,** 1057–1110 (2011).
3. Hasan, M. Z. & Kane, C. L. Colloquium: topological insulators. *Rev. Mod. Phys.* **82,** 3045–3067 (2010).
4. Moore, J. Topological insulators: the next generation. *Nat. Phys.* **5,** 378–380 (2009).
5. Zhang, H. J. *et al.* Topological insulators in Bi_2Se_3, Bi_2Te_3 and Sb2Te3 with a single Dirac cone on the surface. *Nat. Phys.* **5,** 438–442 (2009).
6. Hsieh, D. *et al.* A tunable topological insulator in the spin helical Dirac transport regime. *Nature* **460,** 1101–1105 (2009).
7. Chen, Y. L. *et al.* Experimental realization of a three-dimensional topological insulator Bi_2Te_3. *Science* **325,** 178–181 (2009).
8. Xia, Y. *et al.* Observation of a large-gap topological-insulator class with a single dirac cone on the surface. *Nat. Phys.* **5,** 398–402 (2009).
9. Fu, L., Kane, C. L. & Mele, E. J. Topological insulators in three dimensions. *Phys. Rev. Lett.* **98,** 106803 (2007).
10. Hikami, S., Larkin, A. I. & Nagaoka, Y. Spin-orbit interaction and magnetoresistance in the two dimensional random system. *Prog. Theor. Phys.* **63,** 707–710 (1980).
11. Beenakker, C. W. J. & Houten, H. V. Quantum transport in semiconductor nanostructures. *Solid State Phys.* **44,** 1–228 (1991).
12. Zhang, Y. *et al.* Crossover of the three-dimensional topological insulator Bi_2Se_3 to the two-dimensional limit. *Nat. Phys.* **6,** 584–588 (2010).
13. Cho, S., Butch, N. P., Paglione, J. & Fuhrer, M. S. Insulating behavior in ultrathin bismuth selenide field effect transistors. *Nano Lett.* **11,** 1925–1927 (2011).
14. Linder, J., Yokoyama, T. & Sudbø, A. Anomalous finite size effects on surface states in the topological insulator Bi_2Se_3. *Phys. Rev. B.* **80,** 205401 (2009).
15. Chen, J. *et al.* Gate-voltage control of chemical potential and weak antilocalization in Bi_2Se_3. *Phys. Rev. Lett.* **105,** 176602 (2010).
16. Checkelsky, J. G., Hor, Y. S., Cava, R. J. & Ong, N. P. Surface state conduction observed in voltage-tuned crystals of the topological insulator Bi_2Se_3. *Phys. Rev. Lett.* **106,** 196801 (2010).
17. Kim, Y. S. *et al.* Thickness-dependent bulk properties and weak antilocalization effect in topological insulator Bi_2Se_3. *Phys. Rev. B* **84,** 073109 (2011).
18. He, H.-T. *et al.* Impurity effect on weak antilocalization in the topological insulator Bi2Te3. *Phys. Rev. Lett.* **106,** 166805 (2011).
19. Chen, J. *et al.* Tunable surface conductivity in Bi_2Se_3 revealed in diffusive electron transport. *Phys. Rev. B* **83,** 241304 (2011).
20. Steinberg, H., Laloe, J. B., Fatemi, V., Moodera, J. S. & Jarillo-Herrero, P. Electrically tunable surface-to-bulk coherent coupling in topological insulator thin films. *Phys. Rev. B* **84,** 233101 (2011).
21. Matsuo, S. *et al.* Weak antilocalization and conductance fluctuation in a submicrometer-sized wire of epitaxial Bi_2Se_3. *Phys. Rev. B* **85,** 075440 (2012).
22. Taskin, A. A., Sasaki, S., Segawa, K. & Ando, Y. Manifestation of topological protection in transport properties of epitaxial Bi_2Se_3 thin films. *Phys. Rev. Lett.* **109,** 066803 (2012).
23. Butch, N. P. *et al.* Strong surface scattering in ultrahigh-mobility Bi_2Se_3 topological insulator crystals. *Phys. Rev. B* **81,** 241301 (2010).
24. Kim, D. *et al.* Surface conduction of topological Dirac electrons in bulk insulating Bi_2Se_3. *Nat. Phys.* **8,** 460–464 (2012).
25. Beidenkopf, H. *et al.* Spatial fluctuations of helical Dirac fermions on the surface of topological insulators. *Nat. Phys.* **7,** 939–943 (2011).
26. Adam, S., Hwang, E. H., Galitski, V. M. & Das Sarma, S. A self-consistent theory for graphene transport. *Proc. Natl Acad. Sci. USA* **104,** 18392–18397 (2007).
27. Adam, S., Hwang, E. H. & Das Sarma, S. Two-dimensional transport and screening in topological insulator surface states. *Phys. Rev. B* **85,** 235413 (2012).
28. Garate, I. & Glazman, L. Weak localization and antilocalization in topological insulator thin films with coherent bulk-surface coupling. *Phys. Rev. B* **86,** 035422 (2012).
29. Lu, H. Z., Shi, J. & Shen, S. Q. Competition between weak localization and antilocalization in topological surface states. *Phys. Rev. Lett.* **107,** 076801 (2011).
30. Cha, J. *et al.* Effects of magnetic doping on weak antilocalization in narrow Bi_2Se_3 nanoribbons. *Nano Lett.* **12,** 4355–4359 (2012).
31. Tkachov, G. & Hankiewicz, E. M. Weak antilocalization in HgTe quantum wells and topological surface states: Massive versus massless Dirac fermions. *Phys. Rev. B* **84,** 035444 (2011).
32. Zhu, Z. H. *et al.* Rashba spin-splitting control at the surface of the topological insulator Bi_2Se_3. *Phys. Rev. Lett.* **107,** 186405 (2011).
33. Lang, M. *et al.* Competing weak localization and weak antilocalization in ultrathin topological insulators. *Nano Lett.* **13,** 48–53 (2013).

Acknowledgements

This work was supported by NSF grant number DMR-1105224. Preparation of Bi_2Se_3 was supported by NSF MRSEC (DMR-0520471) and DARPA-MTO award (N66001-09-c-2067). N.P.B. was partially supported by the Centre for Nanophysics and Advanced Materials. M.S.F. acknowledges support from an ARC Laureate Fellowship. D.K. acknowledges useful conversations with Sergey S. Pershoguba.

Author contributions

D.K. fabricated devices, performed the electrical measurements and analysed the data with M.S.F. P.S., N.P.B. and J.P. prepared single crystal Bi_2Se_3 starting material. D.K. and M.S.F. wrote the manuscript with contributions from all authors.

Additional information

Supplementary Information accompanies this paper at http://www.nature.com/naturecommunications

Competing financial interests: The authors declare no competing financial interests.

Reprints and permission information is available online at http://npg.nature.com/reprintsandpermissions/

How to cite this article: Kim, D. *et al.* Coherent topological transport on the surface of Bi_2Se_3. *Nat. Commun.* 4:2040 doi: 10.1038/ncomms3040 (2013).

© 2013 Macmillan Publishers Limited. All rights reserved.